

# Multiple-Input Multiple-Output (MIMO) Channel Measurements for Urban Military Applications

Jerry R. Hampton, A. Roger Hammons Jr., Manuel A. Cruz, Naim M. Merheb, Douglas E. Paunil, and Feng Ouyang

This article presents results from a measurement campaign to characterize the propagation features of a low-rise urban multiple-input multiple-output (MIMO) channel in the military UHF band. The measurements were made with a  $2 \times 3$  MIMO test bed by fixing the transmitter and moving the receiver along predefined straight and L-shaped paths. Measurements are presented that show the statistical characteristics of the channel, the sensitivity of the spatial correlation between adjacent antennas to antenna spacing, and the channel capacity improvement achievable with MIMO. Results show that antennas can be spaced as closely as one-quarter wavelength without incurring a reduction in capacity due to correlation between antennas, a result that has potentially significant practical implications when operating in the military UHF band. Results also show that significant throughput improvement is possible with MIMO in this urban environment and that a reasonable way to approximate MIMO performance is to use Telatar's channel model with an accurate estimate of propagation loss.

## INTRODUCTION

Multiple-input multiple-output (MIMO) communications techniques have been studied extensively for more than a decade and have been demonstrated both theoretically and empirically to be capable of significantly enhancing the quality and capacity of communications in rich scattering environments.<sup>1,2</sup> Although numerous experimental campaigns have been conducted over the years to characterize the propagation characteristics and communications capacities of MIMO channels,<sup>3-9</sup>

an examination of these and similar empirical studies showed that the focus to date has been on commercial applications and has involved geometries and RF frequencies of interest to that community.

In recent years, however, the U.S. military has also recognized the benefits of MIMO techniques and has funded studies to examine the potential of using MIMO schemes to enhance military communications.<sup>10</sup> Despite these efforts, there remains a dearth of published results

that specifically address environments of interest to the military. One area of particular interest to the military is UHF urban propagation, which has grown in importance in recent years as a consequence of the growing focus on military urban warfare. Unlike commercial environments addressed by most of the measurement campaigns in the literature, which focus primarily on 1.8 and 5.2 GHz and often involve use of an elevated radio at one end of each link, military UHF urban communications operate between 225 and 425 MHz and primarily involve ground-to-ground communications where both ends of each link are between 1 and 2 m above the ground. This article reports measurements that were made to characterize the MIMO propagation characteristics in such an environment and then uses those measurements to estimate the potential communications capacity improvement that can be achieved. The measurement campaign described here was conducted in a “low-rise” (one- to three-level buildings) section of Baltimore, Maryland, in June 2007. While not exhaustive, these measurements provide useful empirical results for an environment that has not been sufficiently addressed in the literature. Preliminary results from our study were presented by Hammons et al.<sup>11</sup> and Hampton et al.<sup>12</sup>

## DESCRIPTION OF EXPERIMENT

### Overview

The measurements described in this article were collected using a  $2 \times 3$  MIMO test bed (two transmitter antennas, three receiver antennas) during several days in June 2007 in Baltimore, Maryland. The test area was characterized by flat topography, a rectangular grid street pattern, and predominantly low-rise buildings with heights equal to two to three stories, similar to the heights of buildings encountered in many urban areas of interest to the military. Figure 1 shows a map of the area where the data were collected and illustrates the two types of collection path geometries used. The data were collected using a stationary transmitter test van with two half-wavelength whip antennas and a receiver van that had three antennas identical to those used on the transmitter van. Data were collected as the receiver van traversed different paths in the urban test area, and the location of each van was monitored as a function of time by using the Global Positioning System (GPS). A nominal receiver van speed of 10–15 mph was used. The total transmitter power, which was divided evenly between the two transmitter antennas, was fixed at 5 W, and the RF center frequency of each signal was 425 MHz. The base of each antenna was approximately 2 m above the ground.

As illustrated in Fig. 1, data were collected by using two sets of runs in this study: line-of-sight (LOS) runs and non-LOS (NLOS) runs, also called L-runs. LOS

runs involved driving the receiver van down the same street where the transmitter van was parked. To study the effect of antenna spacing on MIMO performance, different transmitter and receiver antenna spacings were used on different runs. A total of eight LOS runs were conducted in this test with different combinations of transmitter and receiver antenna spacing: 0.25, 0.75, and 1.25 wavelengths. L-runs refer to collection geometries in which the receiver van drove down the same street on which the transmitter van was parked, then turned a corner and proceeded down a cross-street perpendicular to the first street and no longer within the LOS of the transmitter. The corner was measured to be approximately 200 m from the transmitter. Different antenna spacings were also used on the L-runs. A total of 19 L-runs were made with various combinations of antenna spacing chosen from the following set of values: 0.25, 0.5, 0.75, 1.0, and 1.25 wavelengths. (Physical constraints with the antenna mounting prevented the antennas from being placed more closely than 0.25 wavelength.)

### Channel Probe Design

The transmitted signals from the two transmitter antennas consisted of quasi-orthogonal 255-bit quadrature phase-shift keying (QPSK) channel probes at a rate of 50 kilosymbols/s. These probes consisted of quaternary Family A sequences,<sup>13</sup> which have near optimal auto- and cross-correlation properties with respect to the Welch bound. Figure 2 illustrates the frame struc-

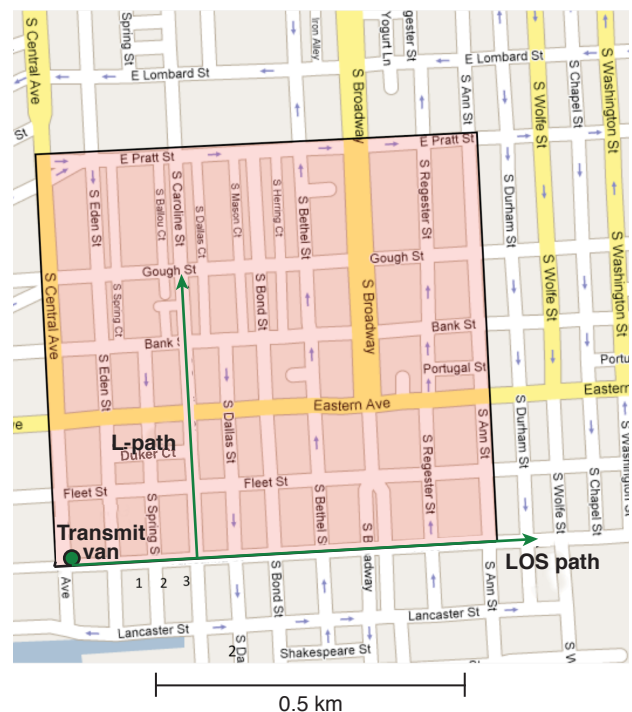


**Figure 1.** Map of the area in Baltimore, Maryland, where testing was performed.

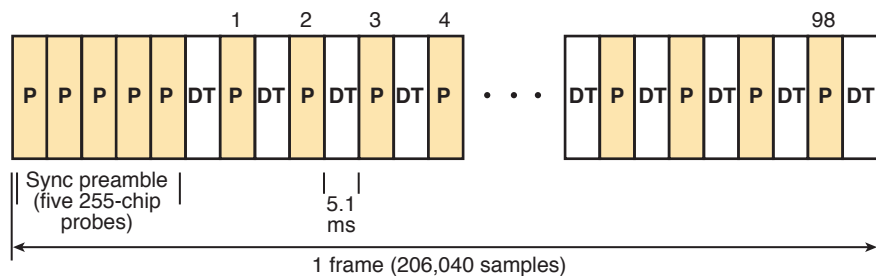


**Figure 2.** Channel probe frame structure used in this study. DT, dead time; P, preamble.

ture of each transmitted signal. The beginning of each frame consisted of a sequence of five 255-symbol probes followed by an alternating sequence of probes and dead times, during which only a carrier was transmitted. This frame structure was repeated during the entire duration of each run. The five-probe preamble was used to estimate the residual carrier frequency in the nominal baseband signal, which was removed before final processing of the data. The channel gain between each pair of transmitter and receiver antennas was estimated from each probe; thus, the MIMO channel transfer matrix was estimated every 5.1 ms during the preamble and every 10.2 ms during the non-preamble portion of each frame. Because only relative signal intensities were used in this study, there was no need to measure the absolute signal power level at the receiver, averting the need for detailed receiver calibration.

## Hardware

Figure 3 shows the transmitter and receiver test vans, and Fig. 4 gives high-level block diagrams of the transmitter and receiver units used in the experiment. The antennas used for the receiver and transmitter arrays were all center-fed, vertically polarized dipoles from Shakespeare Electronic Products Group (model 4310-AT; for details, see <http://shakespeare-military.com/milantennashow.asp?t=89>), providing a gain of approximately 2 dBi (dB isotropically) in the frequency range of 225–470 MHz. The PXI chassis selected from National Instruments (NI) provided all of its modules with a common 10-MHz frequency reference with a skew of less than 250 ps between modules and with common digital triggers with a skew of less than 10 ns between modules. The 10-MHz frequency reference in each chassis was provided by an NI PXI-6608 module with an oven-controlled crystal oscillator with a specified accuracy of 75 parts per billion. Each transmitter chain was composed of an NI PXI-5671 signal generator with digital upconverter connected to a power amplifier (PA). The PAs used were Mini-Circuits model ZHL-5W-1, which are capable of a maximum output power of approximately 37 dBm with a nominal gain of 40 dB (note that the value of 37 dBm actually refers to the minimum 1-dB compres-

sion point of the PA, equaling power  $\sim 5$  W). The transmitter chains, however, were configured such that their outputs did not exceed 35 dBm ( $\sim 3$  W) in order to avoid nonlinearities from the PA. The input to the transmitter channels for channel estimation was a sequence of complex symbols with two samples per symbol, corresponding to a baseband rate of 100

thousand complex samples per second (kCSamples/s). The PXI-5671 digitally interpolated and upconverted the baseband signal to an IF signal sampled at 100 million samples per second (MSamples/s), then performed analog mixing up to the desired carrier frequency. Each receiver chain consisted of an NI PXI-5600 analog downconverter paired with an NI PXI-5142 digitizer with digital downconverter. The analog downconverters each mixed a bandwidth of approximately 20 MHz around the carrier frequency down to an IF of 15 MHz. Each corresponding PXI-5142 digitized the IF signal at a rate of 100 MSamples/s, then digitally downconverted



**Figure 3.** Photos of the transmitter (Tx, upper) and receiver (Rx, lower) vans.

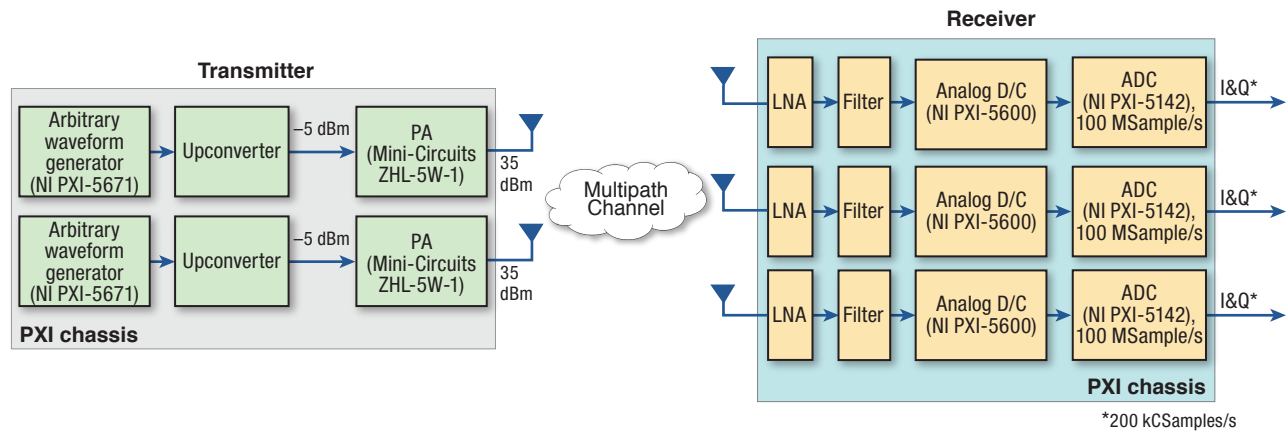


**Figure 4.** High-level system diagram of narrowband MIMO test bed. ADC, analog-to-digital converter; D/C, downconverter; I&Q, in-phase and quadrature-phase components; LNA, low-noise amplifier.

and decimated the sampled signal into a sequence of complex samples (in-phase and quadrature pairs) of the desired baseband rate, which was 200 kCSamples/s for channel estimation. It should be noted that the analog filter bandwidth, intermediate frequency (IF), and the use of an analog-to-digital converter sampling rate of 100 MSamples/s were the result of the decision to use existing test equipment for this study and were not selected by the waveform characteristics used in the testing.

### Signal Processing

The channel transfer matrix,  $\mathbf{H}$ , is the fundamental quantity measured in this study from which all other parameters are derived. In general, for  $M_T$  transmitter antennas and  $M_R$  receiver antennas,  $\mathbf{H}$  is dimensioned  $M_R \times M_T$ , and under the assumption of flat fading, which was assumed to be valid in this study, each element of  $\mathbf{H}$  is a complex phasor with the form  $H_{mn} = |H_{mn}|e^{j\phi_{mn}}$ . Under this assumption, the complex baseband representation of the received signal can be denoted as

$$\mathbf{r} = \mathbf{H}\mathbf{s} + \mathbf{n}, \tag{1}$$

where  $\mathbf{r}$  is a complex  $M_R \times 1$  vector,  $\mathbf{s}$  is the complex baseband transmit signal vector dimensioned  $M_T \times 1$ , and  $\mathbf{n}$  is the  $M_R \times 1$  additive noise vector at the receiver. In this study,  $M_T = 2$  and  $M_R = 3$ . The vector  $\mathbf{s}$  represents the transmitted signal at the output of the baseband portion of the transmitter and  $\mathbf{r}$  represents the received signal at the output of the analog-to-digital converter in the receiver; thus,  $\mathbf{H}$  can be thought of as the effective channel transfer matrix that includes the propagation channel proper as well as all the gains and losses in the IF and RF hardware chains.

Because the probe sequences are known and nearly orthogonal, the individual components  $H_{mn}$  of the channel matrix can be estimated using standard correlation techniques. The primary issue is that the radio

frequency of the received signal is not known exactly because of Doppler and offsets between the transmitter and receiver oscillators. Thus, the frequency offset is estimated first and removed before the channel estimates are derived.

## RESULTS

### Channel Spatial Correlation

Because correlation between signals at different antennas in a MIMO system is an important practical factor that can degrade MIMO system performance, empirical evaluation of spatial correlations was a key objective of the study.

We define  $\rho_r$ , the receive spatial correlation coefficient, as the average magnitude of the complex correlation coefficients between  $H_{mn}$  and  $H_{m+1,n}$ , with the average taken over all transmitter antennas  $n$  and all adjacent receiver antenna pairs  $m, m + 1$ . Similarly,  $\rho_t$ , the transmit spatial correlation coefficient, is defined with respect to adjacent transmitter antenna pairs  $n, n + 1$ . Figure 5 shows plots of  $\rho_r$  versus transmitter-to-receiver distance  $d$  for antenna spacings  $s_{RX} = 0.25, 0.75$ , and  $1.25$  wavelengths  $\lambda$ , where each curve is obtained by averaging over all L-runs. Similar results were obtained for  $\rho_t$ . The results show that both the transmit and the receive spatial correlations are quite small, irrespective of antenna spacing. In general, correlation would be expected to decrease as the antenna spacing increases; however, that trend is not observed in these data over the range of antenna spacings considered. These results show that for the conditions encountered in this study, reducing the spacing between antennas to at least  $\lambda/4$  will not degrade the MIMO performance benefit.

Figures 6–8 provide further insight into this phenomenon. Figures 6 and 7 show typical plots of the squared magnitude of the channel response between a single transmitter and two adjacent receiver antennas

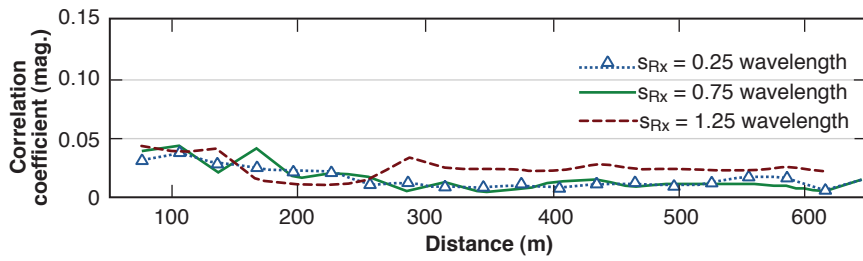


**Figure 5.** The magnitude (mag.) of the receiver complex spatial correlation coefficient averaged over all L-runs for three different receive antenna spacings ( $s_{RX}$ ). The results show consistently low spatial correlation over the range of antenna spacings considered in the study described in this article, implying little MIMO performance degradation even when the spacing is as little as 0.25 wavelength.

spaced at 0.25 and 1.25 wavelengths, respectively. It is clear by inspection that the correlation at 0.25-wavelength spacing is significantly higher than at 1.25 wavelengths; however, this effect is not reflected in Figure 5, which indicates that the spatial correlation coefficient is

as the phase of the channel response, we conclude that it is the poorly correlated nature of the phase that gives rise to the low correlation values observed in Fig. 5. It is important to note that the performance of a MIMO system can be shown to depend on the correlation of the

independent of receiver antenna spacing. To help understand this apparent conflict, consider Fig. 8, which shows the phase of the channel response versus distance for the same data shown in Fig. 6 for a 20-m portion of the path corresponding to  $80 \leq d \leq 100$  m. The phase profiles in Fig. 8 are observed to be poorly correlated, whereas the magnitude of the channel response over the same distance range in Fig. 6 is highly correlated. Because the spatial correlation coefficients in Fig. 5 depend on the amplitude as well

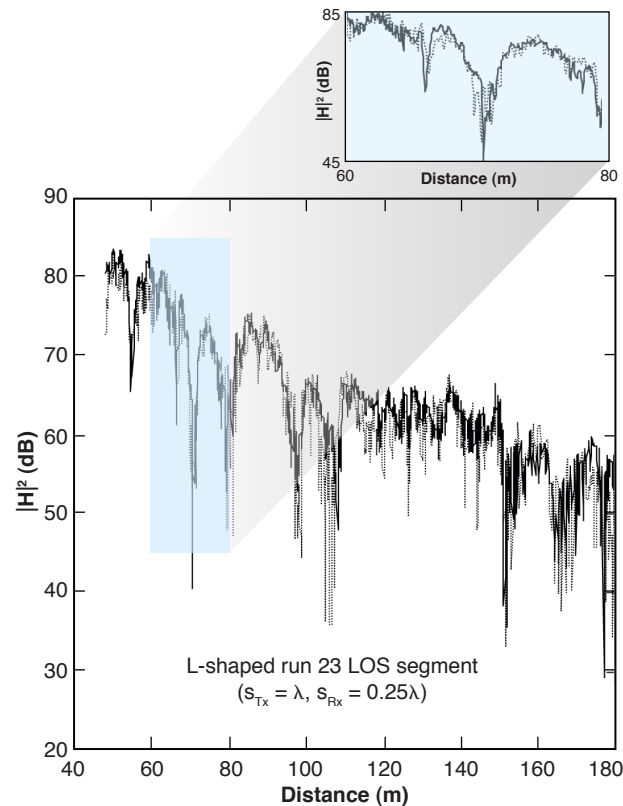


**Figure 6.** Representative plots showing the squared magnitude of the channel responses between transmitter antenna 1 and receiver antennas 2 and 3 when the receiver antenna spacing is 0.25 wavelength. At this close spacing, the magnitudes squared of the channel responses are observed to be highly correlated. The inset shows this correlation in detail for a magnified portion of the plot.

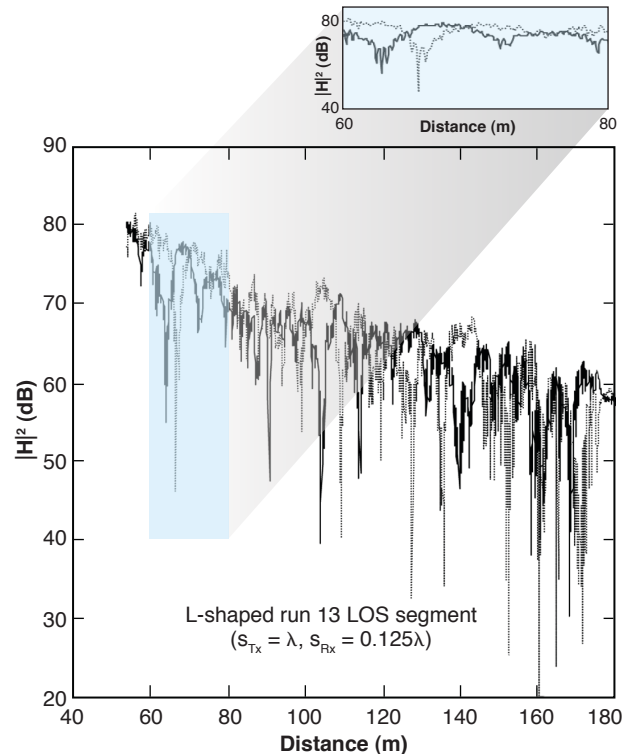


**Figure 7.** Representative plots showing the squared magnitude of the channel responses between transmitter antenna 1 and receiver antennas 2 and 3 when the receiver antenna spacing is increased to 1.24 wavelengths. The correlation (shown in the inset in detail for a magnified portion of the plot) is observed to be much poorer here than that shown in Fig. 6 because the antenna spacing is larger.

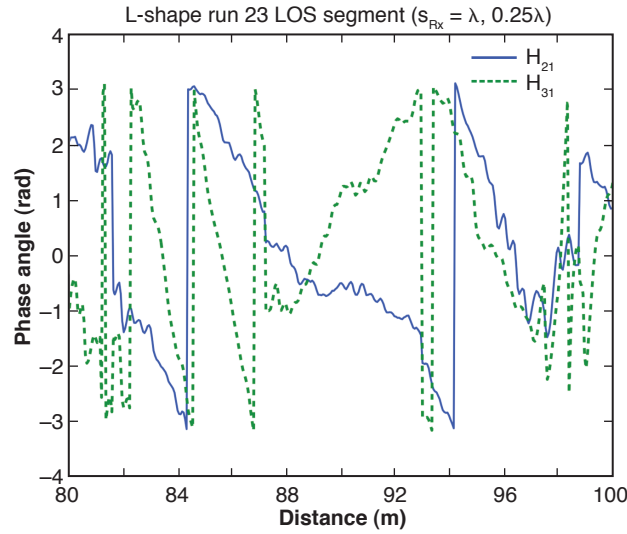


**Figure 8.** Overlay of  $\angle H_{21}(d)$  and  $\angle H_{31}(d)$  for  $80 \leq d \leq 100$  m for the data shown in Fig. 6. This plot shows that the phase responses of the channels between transmitter antenna 1 and receiver antennas 2 and 3 are highly uncorrelated, which helps explain the apparent disparity between the data shown in Figs. 6 and 7 and Fig. 5.

complex channel response, not on the correlation of the magnitude of the response alone.

The lack of sensitivity to antenna spacing observed in this study is consistent with predictions described by Gesbert et al.<sup>14</sup> for the case where the path length is large in comparison with the diameters of the scattering rings around the transmitter and receiver, a geometry that gives rise to the so-called “pinhole” channel. In the urban environment, scattering comes from buildings and objects in the immediate vicinities of the transmitter and receiver, which would be expected to meet the pinhole criterion even at relatively short path lengths. Gesbert et al.<sup>14</sup> argue from theoretical grounds that the physical antenna spacing has limited impact on the capacity when pinhole channel conditions exist. These predictions are consistent with the results in Fig. 5.

### Channel Capacity

The channel transfer matrices were used to estimate the theoretical ergodic MIMO communications capacity as a function of both distance and signal-to-noise ratio (SNR). The approach used was to compute  $\mathbf{H}(d)$ , the channel transfer matrix as a function of distance  $d$ , and to group the data into 20-m bins over which the average propagation loss due to distance was considered constant. As the receiver traversed its route, hundreds of channel matrices were collected for each bin. For each  $3 \times 2$  channel matrix  $\mathbf{H}$ , the instantaneous channel capacity,  $C_{MIMO}$ , was computed by using the following expression (Telatar<sup>2</sup>):

$$C_{MIMO} = \log_2 \left( \det \left( \mathbf{I} + \frac{1}{\sigma^2} \mathbf{H}\mathbf{H}^H \right) \right), \quad (2)$$

where  $\det(\cdot)$  denotes the determinant,  $\mathbf{H}^H$  denotes the Hermitian of  $\mathbf{H}$ ,  $\sigma^2$  is the variance of the Gaussian noise present at each receiver, and  $\mathbf{I}$  denotes an  $M_R \times M_R$  identity matrix. The value of  $\sigma^2$  for each instantaneous capacity value was estimated by computing the variance of the signal in the adjacent dead time in the frame structure and then averaging those values over all six transmit–receive antenna combinations (i.e., T1 to Rx1, Tx1 to Rx2, Tx2 to Rx1, etc., where Tx indicates the transmitter and Rx the receiver antennas). The ergodic capacity in each 20-m bin was computed by averaging the instantaneous capacity values within the bin. For comparison, ergodic capacity for a single-input single-output (SISO) channel was also computed by interpreting each  $3 \times 2$  channel matrix as comprising six SISO realizations. The instantaneous capacity for each SISO realization was computed in accordance with Shannon’s formula, which is obtained from Eq. 2 when the number of antennas at each end of the link is equal to 1:

$$C_{SISO_{mn}} = \log_2 \left( 1 + \frac{|H_{mn}|}{\sigma^2} \right). \quad (3)$$

The ergodic SISO capacity  $C_{SISO}$  in each 20-m bin was computed by averaging  $C_{SISO_{mn}}$  in the bin over all values of  $m$  and  $n$ .

Figures 9 and 10 show representative capacity results for LOS geometry for both the SISO and conventional  $2 \times 3$  MIMO cases. Figure 9 shows measured ergodic capacity (in dB-bits/s per Hz) as a function of distance, while Fig. 10 shows the same data versus SNR. These results demonstrate that MIMO capacities substantially exceed the corresponding SISO capacities. For comparison, the plot versus SNR also shows the corresponding capacity curves due to Telatar<sup>2</sup> for the ideal flat Rayleigh fading channel in which the channel coefficients are independent, identically distributed (i.i.d.) circular complex Gaussian random variables with zero mean and unit variance. The measured capacities are in good agreement with the theoretical model, especially at higher SNRs. Note that Telatar<sup>2</sup> shows that in the limit as SNR approaches infinity, the capacity of an  $M_T \times M_R$  MIMO system in i.i.d. circular complex Gaussian noise will be  $\min\{M_R, M_T\} = 2$  times the capacity of a SISO system with the same SNR. This factor of 2 times performance improvement is evident in the empirical results.

Figures 11 and 12 show analogous results for L-path geometry, where there is an abrupt and substantial SNR drop after the receiver turns the corner, which is indicated by the vertical dashed line. Otherwise, these

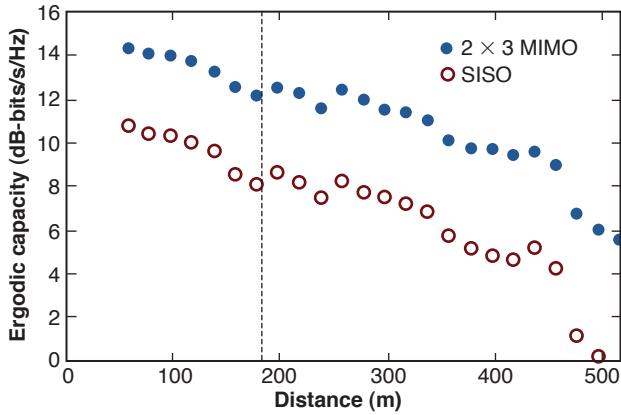


Figure 9. Ergodic capacity versus distance for LOS geometry.

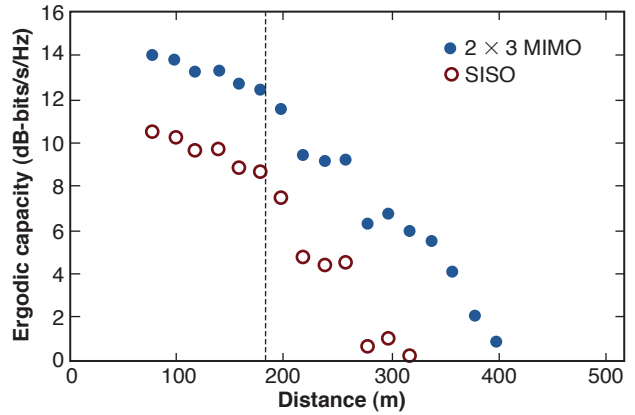


Figure 11. Ergodic capacity versus distance for L-run geometry.

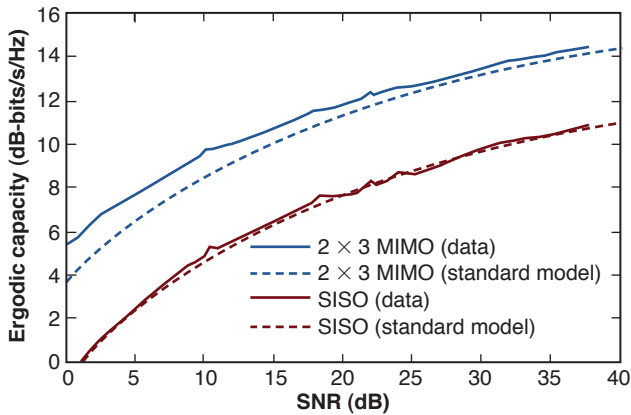


Figure 10. Ergodic capacity versus SNR for LOS geometry.

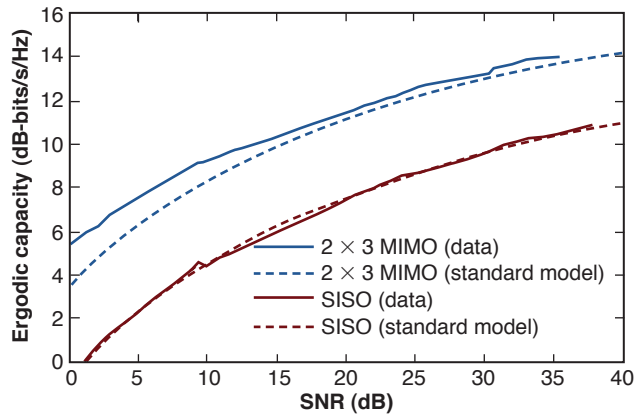


Figure 12. Ergodic capacity versus SNR for L-run geometry.

results are similar to the LOS results. The comparison between the theoretical predictions and the measurements is similar to that for the LOS runs.

### Path Loss

Although the ergodic and outage capacities of a MIMO system are dependent on SNR and the richness of the scattering in environment, the SNR at the receiver depends on the mean path loss as a function of distance between the transmitter and the receiver. Thus, it is important for the system designer to have accurate propagation models for the operating conditions of interest.

In a previous study, Hampton et al.<sup>15</sup> performed a measurement campaign to characterize the propagation loss in an urban canyon environment between ground-based communicators in the same frequency band used in this study. A simple empirical model was developed from the measurements in that study for the mean path loss as a function of distance on L-path links. Because the present study was conducted in the same frequency band as that previous study but in a low-rise urban environment with two- to three-level buildings (compared

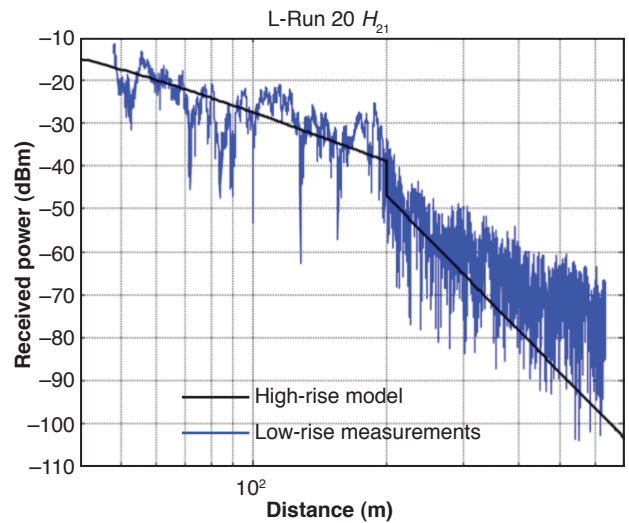


Figure 13. Example illustrating the comparison of the high-rise model prediction (black curve) with the low-rise measurements (blue curve).

with building heights of 30–60 m in the Hampton et al.<sup>15</sup> study), it is possible to gain some insight into the impact that building height has on propagation loss by comparing the results of these two studies.

Figure 13 is a representative plot of received signal strength versus distance for an L-path run from the present study (blue curve). Superimposed on this plot in black is a curve of the predicted mean received power level, based on the empirical model described by Hampton et al.<sup>15</sup> for a high-rise urban environment. These plots show that in the LOS region, the average received power level decreases with distance at about the same rate for both high-rise and low-rise environments. After turning the corner (at  $d = 200$  m), however, the received power in the low-rise environment decreased less rapidly with distance than did the predicted high-rise rate. Hampton et al.<sup>15</sup> showed that the received power decreases with distance after the corner as  $d^{-m_{\text{NLOS}}(d_c, f, w)}$ , where the exponent depends on the distance to the corner  $d_c$ , the RF frequency  $f$ , and the street width  $w$ . In the present study,  $d_c \approx 200$  m,  $f = 425$  MHz, and  $w = 21$  m, which results in  $m_{\text{NLOS}} = 9.8$  in the urban canyon environment (i.e., 30- to 60-m building heights). In contrast, the average exponent value for the present study in a low-rise environment was found to be 5.4. These results, while limited in scope, demonstrate the importance of building height to path loss; building height is thus an important factor that needs to be considered when designing a MIMO system in an urban environment.

## CONCLUSIONS

This article presents results from a measurement campaign conducted to characterize the propagation features of a low-rise urban MIMO channel in the military UHF band. A  $2 \times 3$  MIMO test bed was used to collect data by fixing the transmitter and moving the receiver along predefined straight and L-shaped paths.

The study examined the sensitivity of antenna spatial correlation to the spacing between adjacent antennas. Transmit and receive spatial correlation coefficients were shown to remain small even when the antenna spacing was only  $\lambda/4$ . By separately examining the correlations of the amplitudes and phases of the channel responses, it was shown that the low spatial correlation values are driven by the phase properties of the channel, which were found to be highly uncorrelated. These results have important practical implications for military UHF MIMO systems, because they suggest that antennas in urban environments can be placed closer together than the common  $\lambda/2$  rule of thumb. This is particularly significant when operating at low UHF frequencies, where wavelengths are relatively large.

Channel measurements from this study were also used to examine the potential capacity increase that can be achieved through MIMO techniques. Ergodic capacity was computed as a function of distance for both MIMO and SISO channels and compared with theoretical predictions assuming i.i.d. circular complex Gaussian

channels. The results showed that the measurements and theory were in close agreement and that, at high SNR, the  $2 \times 3$  MIMO capacity was approximately twice as large as that of the corresponding SISO system, in concert with theoretical asymptotic predictions.

Our results suggest that a reasonable first approximation of MIMO performance in urban settings is the standard Telatar channel model, together with an accurate model of propagation loss in such environments.

## REFERENCES

- Foschini, G., "Layered Space-Time Architecture for Wireless Communication in a Fading Environment When Using Multi-Element Antennas," *Bell Labs Tech. J.* 1(2), 41–59 (1996).
- Telatar, E., "Capacity of Multi-Antenna Gaussian Channels," *Eur. Trans. Telecommun.* 10(6), 585–595 (1999).
- Wallace, J. W., Jensen, M. A., Swindlehurst, A. L., and Jeffs, B. D., "Experimental Characterization of the MIMO Wireless Channel: Data Acquisition and Analysis," *IEEE Trans. Wireless Commun.* 2(2), 335–343 (2003).
- Chua, H. Y. E., Sakaguchi, K., and Araki, K., "Experimental and Analytical Investigation of MIMO Channel Capacity in an Indoor Line-of-Sight (LOS) Environment," in *Proc. 15th IEEE International Symp. on Personal, Indoor and Mobile Radio Communications (PIMRC 2004)*, Barcelona, Spain, vol. 1, pp. 295–300 (2004).
- Garcia-Garcia, L., Jalden, N., Linkmark, B., Zetterberg, P., and De Haro, L., "Measurements of MIMO Capacity at 1800 MHz with In- and Outdoor Transmitter Locations," in *Proc. European Conf. on Antennas Propagation (EuCAP 2006)*, Nice, France, paper 36933 (2006).
- Alatossava, M., Holappa, V.-M., and Ylitalo, J., "Outdoor to Indoor MIMO Radio Channel Measurements at 5.25 GHz—Characterization of Propagation Parameters," in *Proc. European Conf. on Antennas Propagation (EuCAP 2006)*, Nice, France, paper 346886 (2006).
- Chizhik, D., Ling, J., Wolniansky, P. W., Valenzuela, R. A., Costa, N., and Huber, K., "Multiple-Input-Multiple-Output Measurements and Modeling in Manhattan," *IEEE J. Selected Areas Commun.* 21(3), 321–331 (2003).
- Yu, K., Bengtsson, M., Ottersten, B., McNamara, D., Karlsson, P., and Beach, M., "Second Order Statistics of NLOS Indoor MIMO Channels Based on 5.2 GHz Measurements," in *Proc. IEEE Global Telecommunications Conf. 2001 (GLOBECOM '01)*, San Antonio, TX, vol. 1, pp. 156–160 (2001).
- Jaramillo, R. E., Fernández, O., and Torres, R. P., "Empirical Analysis of a  $2 \times 2$  MIMO Channel in Outdoor-Indoor Scenarios for BFWA Applications," *IEEE Antennas Propag. Mag.* 48(6), 57–69 (2006).
- Fox, N., Wampler, J., Lai, H.-Q., and Morris, D., "Communication Advantages with Mobile Network Multiple-Input Multiple-Output (MIMO) (MNM) Technology," *Proc. Military Communications Conf. (MILCOM 2010)*, San Diego, CA (2010) (unclassified version available from the author by request).
- Hammons, A. R., Hampton, J., Merheb, N., and Cruz, M., "Cooperative MIMO Field Measurements for Military UHF Band in Low-Rise Urban Environment," in *Proc. IEEE Sensor Array and Multichannel Signal Processing Workshop*, Darmstadt, Germany, pp. 122–126 (2008).
- Hampton, J. R., Cruz, M. A., Merheb, N. M., Hammons, A. R., Paunil, D. E., and Ouyang, F., "MIMO Channel Measurements for Urban Military Applications," in *Proc. Military Communications Conf. (MILCOM 2008)*, San Diego, CA, pp. 1–7 (2008).
- Boztas, S., Hammons, R., and Kumar, P. V., "4-Phase Sequences with Near-Optimum Correlation Properties," *IEEE Trans. Information Theory* 38(3), 1101–1113 (1992).
- Gesbert, D., Bolcskei, H., Gore, D. A., and Paulraj, A. J., "Outdoor MIMO Wireless Channels: Models and Performance Prediction," *IEEE Trans. Commun.* 50(12), 1926–1934 (2002).
- Hampton, J. R., Merheb, N. M., Lain, W. L., Paunil, D. E., Shuford, R. M., and Kasch, W. T., "Urban Propagation Measurements for Ground Based Communication in the Military UHF Band," *IEEE Trans. Antennas Propag.* 54(2), 644–654 (2006).

# The Authors



Jerry R. Hampton

A. Roger  
Hammons Jr.

Manuel A. Cruz



Naim M. Merheb



Douglas E. Paunil



Feng Ouyang

**Jerry R. Hampton** was the technical lead on the study described in this article and is an APL Principal Professional Staff member. He is a communication systems engineer and section supervisor specializing in wireless communications. **A. Roger Hammons Jr.** was the Principal Investigator for the Independent Research and Development study on MIMO communications that funded this work. His research areas include space-time code design, information theory, and wireless communications. He is the Assistant Group Supervisor for APL's Communication and Networking Technology Group. **Manuel A. Cruz** is a communication systems engineer focusing on RF propagation, assessing wireless communication system jamming vulnerabilities, and computational electromagnetics. He performed most of the data processing in this study. **Naim M. Merheb** is a communication systems engineer with extensive experience in testing instrumentation and in conducting testing and evaluation of communication systems. He was responsible for the testing instrumentation in this study. **Douglas E. Paunil** is a project manager and systems engineer, and he supports a variety of communication testing and evaluation activities. He was responsible for designing the support structures for the antennas on the two test vans in this experiment. **Feng Ouyang** has extensive experience designing and analyzing communication systems by using mathematical and computer simulation techniques. He supported this study by participating in the collection of the data and by serving as a technical consultant during the processing and analysis of the measurements. All of the authors are members of the Communication and Networking Technology Group of APL's Applied Information Sciences Department. For further information on the work reported here, contact Jerry Hampton. His e-mail address is [jerry.hampton@jhuapl.edu](mailto:jerry.hampton@jhuapl.edu).

The Johns Hopkins APL Technical Digest can be accessed electronically at [www.jhuapl.edu/techdigest](http://www.jhuapl.edu/techdigest).